Thermal-hydraulic Assessment of the Proposed NIST Neutron Source Design

Anil Gurgen*, Abdullah G. Weiss, and Joy S. Shen†
NIST Center for Neutron Research
100 Bureau Drive, Gaithersburg, MD 20899, USA
anil.gurgen@nist.gov; abdullah.weiss@n ist.gov; joy.shen@nist.gov

doi.org/10.13182/NURETH20-40169

ABSTRACT

To replace the ageing reactor at the NIST Center for Neutron Research, a new reactor design is proposed, namely the NIST Neutron Source or NNS. The NNS will contain a light-water moderated and cooled core that would serve as a neutron source for a state-of-the-art facility for neutron scattering and irradiation experiments to the domestic and international scientific community. The core is planned to use a 3x3 rectangular core fueled with low-enriched U-10Mo curved plates with aluminum cladding, where each assembly contains 21 plates, yielding a total of 64 coolant channels in each row in the core. This work details the development of a custom thermal-hydraulics analysis model capable of computing flow rates and axial temperature distributions of the coolant, the cladding, and the fuel. Analyses include temperature distributions, and thermal limits such as the Critical Heat Flux Ratio (CHFR) and the Onset of Flow Instability Ratio (OFIR). This work also discusses how the operation parameters affect the temperature fields and thermal limits of the NNS.

KEYWORDS
Thermal; Hydraulics; NNS; Sensitivity; Uncertainty

1. INTRODUCTION

The preconceptual design of a new reactor at the National Institute of Standards and Technology (NIST) Center for Neutron Research (NCNR) is currently being pursued in an effort to eventually replace the existing National Bureau of Standards Reactor (NBSR). The new reactor, named the NIST Neutron Source (NNS), is proposed as a pool-type reactor with forced upflow convection of the primary light-water coolant in the core [1]. The NNS core, shown in Figure 1, is a 20-MW_{th} light-water cooled and moderated compact core that favors maximum neutron leakage for out-of-core neutron scattering experiments. The current core design is fueled with U-10Mo high-assay LEU plate fuel assemblies in a 9x9 square lattice configuration. Each row in the core (Figure 1) contains 64 coolant channels, 60 of which are bounded by two fuel plates, 2 are bounded by walls in fuel assemblies, and 2 are bounded by chimney walls containing the entire core. Note that the core also contains channels in the control and safety shim blades bounding boxes (separating each of the rows in the core), and there are also channels

* Additional affiliation: Department of Materials Science and Engineering, University of Maryland, College Park, MD 20742, USA
† Additional affiliation: Department of Mechanical Engineering, University of Maryland, College Park, MD 20742, USA

that hold burnable cadmium poison wires. The shim blades and cadmium poison channels are not considered in this work, and they are the subject of future investigations.

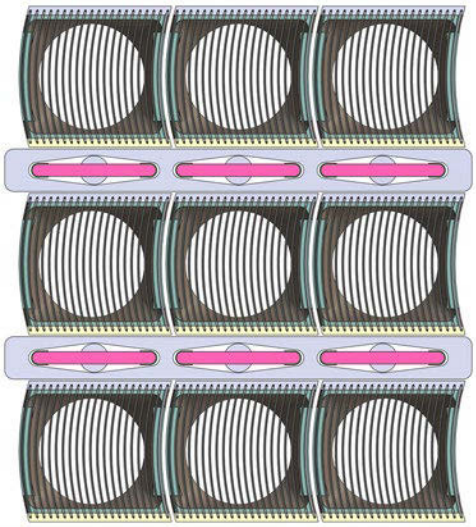

Figure 1. A top view of the NNS core

This work focuses on the behavior of the 64 fuel channels, and follows up on previous works [2, 3] by adding the contributions from heat conduction in the fuel plates to the thermal-hydraulics solution. This paper describes the analysis methodology and the custom computational framework utilized for modeling the thermal-hydraulics behavior in the NNS. The results show the axial temperature distributions for the fuel meat, cladding, and the coolant at various cycle states of the NNS. The previous work [2] models the thermal-hydraulics characteristics of the NNS by assuming equal heat flux at both sides of the fuel plates. There are CFD modeling efforts [4] to better characterize the inlet plenum physics of the NNS, and the current CFD models are based on the assumption of equal heat flux at both sides of the fuel plates. This work is also aimed to assess the uncertainty that the equal heat flux assumption causes in the thermal-hydraulics analysis.

2. METHODOLOGY

Thermal-hydraulic analysis of the NNS is done with in-house thermal-hydraulics solver. The solver is written in MATLAB/Simulink® R2022a version. The fuel plates are curved; therefore, the coolant channel parameters such as flow areas, wetted perimeters, heated perimeters and hydraulic diameters are calculated by accounting the curved nature of the fuel plates and coolant channels. This model accounts for temperature variations in each of the channels by invoking temperature-dependent properties described by functions obtained from literature [5]. The utilized temperature-dependent relations for the thermophysical properties of the coolant are presented in Equations 1-5 for thermal conductivity (k in W/m-K), specific heat (c_p in kJ/kg-K), mass density (ρ in kg/m^3), dynamics viscosity (μ in Pa-s), and saturation temperature (T_{sat} in ℃). In equations (1) – (5), the coolant temperature (T_∞) and pressure (P_∞) are in units of ℃ and MPa, respectively.

$$k = 0.568 + (1.877\,T_\infty \times 10^{-3}) - (8.179\,T_\infty^2 \times 10^{-6}) + (5.663\,T_\infty^3 \times 10^{-9}) \quad (1)$$

$$c_p = \sqrt{\frac{17.489 - 0.0319\,T_\infty}{1 - (1.675\,T_\infty \times 10^{-3}) - (2.875\,T_\infty^2 \times 10^{-6})}} \quad (2)$$

$$\rho = 1004.789 - 0.046\,T_F - (7.974\,T_F^2 \times 10^{-4}), \qquad T_F = 1.8\,T_l + 32 \quad (3)$$

$$\mu = exp\left(\frac{-6.325 - 0.089\,T_\infty}{1 + (8.705\,T_\infty \times 10^{-3}) - (9.657\,T_\infty^2 \times 10^{-7})}\right) \quad (4)$$

$$T_{sat} = \frac{179.96 + 24.228 \cdot ln(P_\infty)}{1 - 0.106\ln(P_\infty) + (2.951\ln^2(P_\infty) \times 10^{-4})} \quad (5)$$

The solver is a combination of modeling the heat conduction in fuel elements, the heat transfer to liquid coolant, and the coolant fluid mechanics. The following sections briefly mention the utilized equations and correlations for each model.

2.1. Heat Conduction in the Fuel Plate

The heat conduction in the fuel plate is solved with a 1D steady state conduction equation by ignoring the axial and tangential heat conduction. Along the radial direction, the fuel plate has 3 layers. The first and third layers are cladding wall, and the second layer constitutes the fuel meat. The heat conduction equation for the fuel plate can be written as shown in equation (6).

$$\frac{d}{dx}\,k_f\,\frac{d\,T_f(x)}{dx} + q''' = 0 \quad (6)$$

Despite the fuel plates being curved, the heat conduction equation is solved using cartesian coordinates. The difference between solving the heat conduction equation with cartesian and cylindrical coordinates is $0.06\ C°$ for nominal conditions of the NNS. To simplify the model development, solution of heat conduction equation in cartesian geometries is implemented in the solver. For a single fuel plate, the coolant flow velocities on both sides of the plate are different; therefore, the heat flux and clad wall temperatures are different. The developed conduction model calculates the average and maximum fuel temperature. With T_{fi} being the fuel meat temperature at the inner arc, and T_{fo} being the fuel meat temperature at the outer arc, the average fuel temperature can be calculated using equation (7).

$$\overline{T_f} = \frac{T_{fo} + T_{fi}}{2} + \frac{q'''\delta_f^2}{12k_f} \quad (7)$$

Per equation (7), $\overline{T_f}$ is the average fuel temperature, q''' is the volumetric heat generation, δ_f is the fuel meat thickness and k_f is the fuel conductivity. Similarly, the maximum fuel meat temperature can be found via the maxima of the temperature distribution. The location where the maximum fuel temperature occurs is given by equation (8), which allows for the computation of the maximum fuel temperature per equation (9).

$$x_{max} = \frac{k_f(T_{fo} - T_{fi})}{q'''(x_{fo} - x_{fi})} + \frac{{x_{fo}}^2 - {x_{fi}}^2}{2\delta_f} \tag{8}$$

$$T_{f,max} = T_{fi} - \frac{q'''({x_{max}}^2 - {x_{fi}}^2)}{2k_f} + \left((T_{fo} - T_{fi}) + \frac{q'''({x_{fo}}^2 - {x_{fi}}^2)}{2k_f}\right)\frac{x_{max} - x_{fi}}{x_{fo} - x_{fi}} \tag{9}$$

The cladding wall temperature (T_w) for the any side of the fuel plate is calculated by solving the 1D conduction equation without volumetric heat generation. It is calculated with equation (10) where q'' is wall heat flux, δ_c is cladding thickness and k_c is cladding conductivity.

$$T_w = T_f - \frac{q''\,\delta_c}{k_c} \tag{10}$$

The thermal conductivity of the fuel and cladding are temperature dependent. The conductivity of the fuel meat and cladding [6,7] are calculated using the following correlations in equations (11-12) where the conductivity is in units of $W/(m.K)$ and temperature is in units of K.

$$k_f = 0.0413T + 0.1621 \tag{11}$$

$$k_c = -1.73 \times 10^{-7}T^3 + 2.66 \times 10^{-5}T^2 + 0.16T + 120.6 \tag{12}$$

2.2 Heat Transfer to Liquid Coolant

Heat transfer to liquid coolant is single-phase convective heat transfer and is solved with Newton's law of heat transfer given by equation (13).

$$q'' = h(T_w - T_b) \tag{13}$$

Per equation (13), h is the heat transfer coefficient and calculated using a Nusselt number (*Nu*) correlation where the Petukhov-Kirillov correlation [8] is adopted per equation considering its applicability to the rectangular channels. The *Nu* is a function of Reynolds number (*Re*), Prandtl number (*Pr*), and the fanning friction factor (f_T) calculated by equations (14-15).

$$Nu = \frac{Re \cdot Pr \cdot f_T/2}{12.7\sqrt{\frac{f_T}{2}}\,(Pr^{2/3} - 1) + 1.07} \tag{14}$$

$$f_T = (3.64\ln(Re) - 3.28)^{-2} \tag{15}$$

The coolant temperature field is calculated by solving the general energy equation for steady-state, single-phase flow. The simplified approximation to the energy equation is given by equation (16).

$$\rho c_p v \frac{dT}{dz} = -\nabla . \vec{q}'' \tag{16}$$

For a given mass flow rate of the channel, the solver solves the energy equation to calculate the coolant temperature field and calculates the channel heat transfer coefficient using equation and temperature field of the cladding and fuel using the heat conduction equation. Then the coolant temperature field is updated with the calculated channel heat transfer coefficients. The iterations are continued until the convergence is achieved and the calculated temperature fields of coolant, cladding and fuel are reported.

2.3 Coolant Fluid Mechanics

The velocity and pressure distributions in the coolant channels are calculated by solving the conservation of momentum equation. Despite the determination of velocity and pressure field in coolant requires simultaneous solution of the conservation of energy equation as well, the thermal model is separated from the calculation of velocity and pressure distributions. For steady-state calculation, the mass flow rate is constant along the channel and the velocity field is calculated considering the density field of the coolant.

The developed solver is not intended to solve the exact pressure distribution in the coolant channels. It is in interest to calculate the total pressure drop at each channel so that the mass flow rate distribution of the core can be approximated by balancing the total pressure drop for each channel. The model calculates the total pressure drop at each channel which is derived from the steady-state, single-phase momentum equation. The total pressure drop is calculated by equation (17).

$$\Delta P = \sum f_h \cdot \frac{dz}{D_h} \cdot \frac{u_{i,j}^2}{2} \cdot \rho_{i,j} + \sum K_{ent} \cdot \frac{u_{i,1}^2}{2} \cdot \rho_{i,1} + \sum K_{out} \cdot \frac{u_{i,end}^2}{2} \cdot \rho_{i,end} + \sum dz \cdot g \cdot \rho_{i,j} \tag{17}$$

The pressure drop equation takes channel entrance and exit losses into account with form loss coefficients (K_{ent} and K_{out}). It is assumed in this work that the form loss coefficients are 0.5 and 1.0 respectively. The friction factor, f_h, is calculated using the Churchill formula [9]. The Churchill formula is selected because it can capture a wide range of flow conditions, which is desirable considering the early design phase of the NNS. The Churchill friction factor formula is given by equation (18).

$$f_h = 2\left[\left(\frac{8}{Re}\right)^{12} + \frac{1}{(a+b)^{3/2}}\right]^{1/12} \tag{18}$$

Per equation (18), the coefficients a and b can be computed per equation (19). Note that the current cladding material of the NNS is Aluminum 6061. Considering the smoothness of the material [10], the relative roughness of the channel walls is assumed to be $\epsilon/D_h = 10^{-5}$.

$$\begin{cases} a = \left(2.457 \ln\left[\dfrac{1}{\left(\frac{7}{Re}\right)^{0.9} + 0.27\left(\frac{\epsilon}{D_h}\right)}\right]\right)^{16} \\ b = \left(\dfrac{3.753 \times 10^4}{Re}\right)^{16} \end{cases} \tag{19}$$

2.4 Solution Framework

The developed thermal-hydraulic code solves the heat conduction in fuel plate, heat transfer to liquid coolant and coolant fluid mechanics iteratively. At each iteration, the temperature field of the coolant, cladding and fuel are calculated for given mass flow rate of each channel. Then the mass flow rate distribution is calculated considering the pressure drop at each channel with the updated values of the temperature fields. The iterations are continued until the inlet and outlet mass flow rates are converged to the pre-defined input value. The calculation scheme is identical to previous works [2, 3], and it is briefly given in Figure 2.

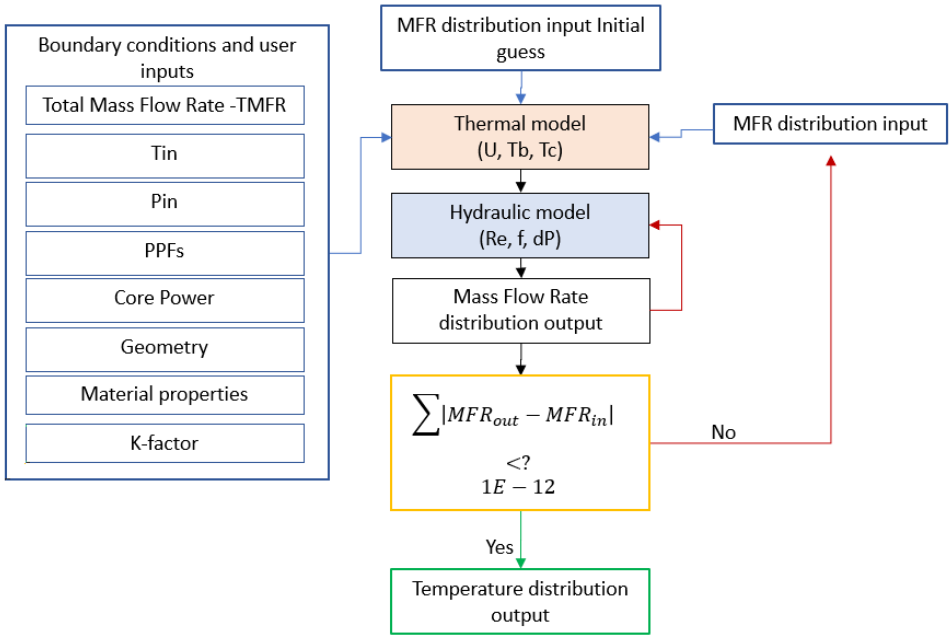

Figure 2. The computational scheme for the coupled thermal-hydraulics model [2]

It must be noted here that fuel meat temperature calculation is added in this updated version of the code, but this addition doesn't affect the overall solution strategy.

2.5 Thermal limits

The general guidance of thermal limits for non-power reactors are 2.0 for minimum Critical Heat Flux Ratio (mCHFR) and minimum Onset of Flow Instability Ratio (mOFIR) [11]. For CHFR, Sudo-Kaminaga [12] correlations are used. The correlations are mass flux and flow direction dependent which separates the flow into three regions, based on the dimensionless mass flux G^*. The three mass flux regions are characterized by a dimensionless mass flux, which is given by,

$$G^* = \frac{G}{\sqrt{\lambda\, g\, \rho_g\, (\rho_l - \rho_g)}} \tag{20}$$

where λ is the critical wavelength defined as,

$$\lambda = \sqrt{\frac{\sigma_\infty}{g\left(\rho_l - \rho_g\right)}} \tag{21}$$

In these equations, G is mass flux ($kg/m^2.s$), σ is surface tension (N/m), ρ_g and ρ_l are density of gas and liquid (kg/m^3) and g is the acceleration of gravity (m/s^2). At the operating regime of the NNS, the critical heat flux (q''_{CHF}) is predicted by Equation (22), and the CHFR is the ratio of q''_{CHF} and local heat flux.

$$q''_{CHF} = 0.7\frac{A_{flow}}{A_{heat}}\frac{\sqrt{w/\lambda}}{\left(1+\sqrt[4]{\rho_g/\rho_l}\right)^2}h_{fg}\sqrt{\lambda\, g\left(\rho_l-\rho_g\right)\rho_g} \tag{22}$$

The OFIR is a measure of local heat flux proximity to the heat flux when the onset of net vapor generation is observed, at which point the onset of nucleate boiling has been surpassed and significant voiding is experienced. The Saha-Zuber criteria[13] is utilized for the OFIR computation, where the heat flux at the onset of net vapor generation (q''_{ONV}) is computed per equation (23), where Pe is the Peclet number and St is the Stanton number such that $Pe = Re \cdot Pr$ and $St = Nu/Pe$. Upon obtaining the appropriate q''_{ONV}, the OFIR is computed with the ratio of q''_{ONV} and local heat flux. The OFIR and CHFR both serve as the thermal-hydraulics limits and can influence design choices considerably. However, it is important to first verify the models and ensure numerical stability, which is the subject of the next section.

$$q''_{ONV} = \begin{cases} 0.0065\ \dfrac{\dot{m}\ c_p(T_{sat}-T_\infty)}{A_{flow}}, & Pe \le 70{,}000 \\ 455\dfrac{k\ (T_{sat}-T_\infty)}{D_h}, & Pe > 70{,}000 \end{cases} \tag{23}$$

3. RESULTS

The boundary conditions and user inputs are given in Table I. This work is an extension of [2] which is tested for accuracy and stability and validated with testing the energy balance at a uniform power density. Therefore, the initial and boundary conditions are kept the same.

The calculations are done for 4 different core states, namely startup (SU), beginning of cycle (BOC), middle of cycle (MOC), and end of cycle (EOC). At the nominal conditions given in Table I, the comparison of the results for temperature fields and thermal limits are given in Table II where $T_{b,max}$ is maximum bulk temperature and $T_{c,max}$ is hottest wall temperature.

The results given in Table II shows that the addition of heat conduction in fuel plate slightly changed the temperature field and thermal limits estimations. The mean absolute percentage difference for the new solver compared to old one is 0.29% for $T_{b,max}$, 0.74% for $T_{c,max}$, 1.73% for $mCHFR$ and 1.85% for mOFIR over all core states. This gives evidence to the CFD models that the assumption of equal heat flux for both sides of the fuel plates are acceptable for steady state analysis of the NNS.

Table I. Boundary conditions and user inputs [2]

Parameter	Value	Units
Core thermal power	20	MW
Total mass flow rate	540	kg/s
Bypass percentage	10	%
Coolant inlet temperature	316.5	K
Side channel window K factor	0.5	–
Inlet K factor	0.5	–
Outlet K factor	1.0	–
Pressure convergence rate	10^{-13}	MPa
Mass flow rate convergence criteria	10^{-12}	kg/s
Friction correlation	Churchill [9,10]	–
Nusselt number correlation	Petukhov & Kirillov [8]	–
Power density distribution	MCNP Model [14]	–
Power peaking factor	MCNP Model [14]	–

Table II. Mean values of maximum temperatures with their uncertainty

Core state	**Without conduction solver**				**With conduction solver**			
	$T_{b,max}\ (K)$	$T_{c,max}\ (K)$	$mCHFR$	$mOFIR$	$T_{b,max}\ (K)$	$T_{c,max}\ (K)$	$mCHFR$	$mOFIR$
SU	332.5	360.9	2.22	12.92	332.0	358.2	2.18	13.25
BOC	332.4	360.5	2.18	13.63	331.6	358.3	2.13	13.88
MOC	332.9	358.4	2.42	15.21	330.4	354.6	2.37	15.43
EOC	329.8	355.0	2.61	15.17	329.7	353.1	2.59	15.41

To account for the effects of deviations from the nominal conditions, the cumulative distribution functions (CDF) of CHFR, OFIR, and temperature fields are computed by running the solver multiple times with different boundary conditions. For the uncertainty analysis, core thermal power, total mass flow rate and core inlet temperature are defined as a random variable with a defined probability distribution. A Monte-Carlo method was then used to combine the probability distributions to calculate CDFs of temperature fields and thermal limits. The probability distributions of core thermal power, total mass flow rate, and core inlet temperature are calculated considering the past operational data of the NBSR. Sources of uncertainties follow a normal distribution, and actual readings of sources of uncertainties are collected and normalized so that their mean value is one. Then the calculated standard deviations are used to generate the probability distributions of sources of uncertainties in the NNS temperature distribution and thermal limits calculation.

The uncertainty bounds are calculated considering a 95/95 criteria which implies that 95% of the sample is within the uncertainty bounds with a probability equal to 95%. The uncertainty limits can be defined as $\mu \pm K\sigma$ where μ is the mean of the sample, σ is the standard deviation of the sample, and K is the tolerance parameter. For 10,000 simulations, K is found to be 1.988 [15]. The mean values and uncertainty bounds of maximum coolant, cladding wall and fuel temperatures are given in Table III.

Table III. Mean values of maximum temperatures with their uncertainty

Core State	Max $T_{coolant}$ (K)	Max T_{wall} (K)	Max T_{fuel} (K)
SU	332.06 ± 1.41	358.67 ± 3.32	377.84 ± 4.73
BOC	331.62 ± 1.38	358.81 ± 3.34	378.31 ± 4.77
MOC	330.49 ± 1.30	355.02 ± 3.06	372.80 ± 4.36
EOC	329.77 ± 1.25	353.50 ± 2.94	370.14 ± 4.16

BOC is a slightly more limiting core state with higher mean maximum cladding wall temperature and maximum fuel temperature. The axial distributions of bulk coolant temperature, maximum cladding wall temperature and maximum fuel temperature are given in Figure 3 with uncertainty bounds, for the hottest channel at the BOC state.

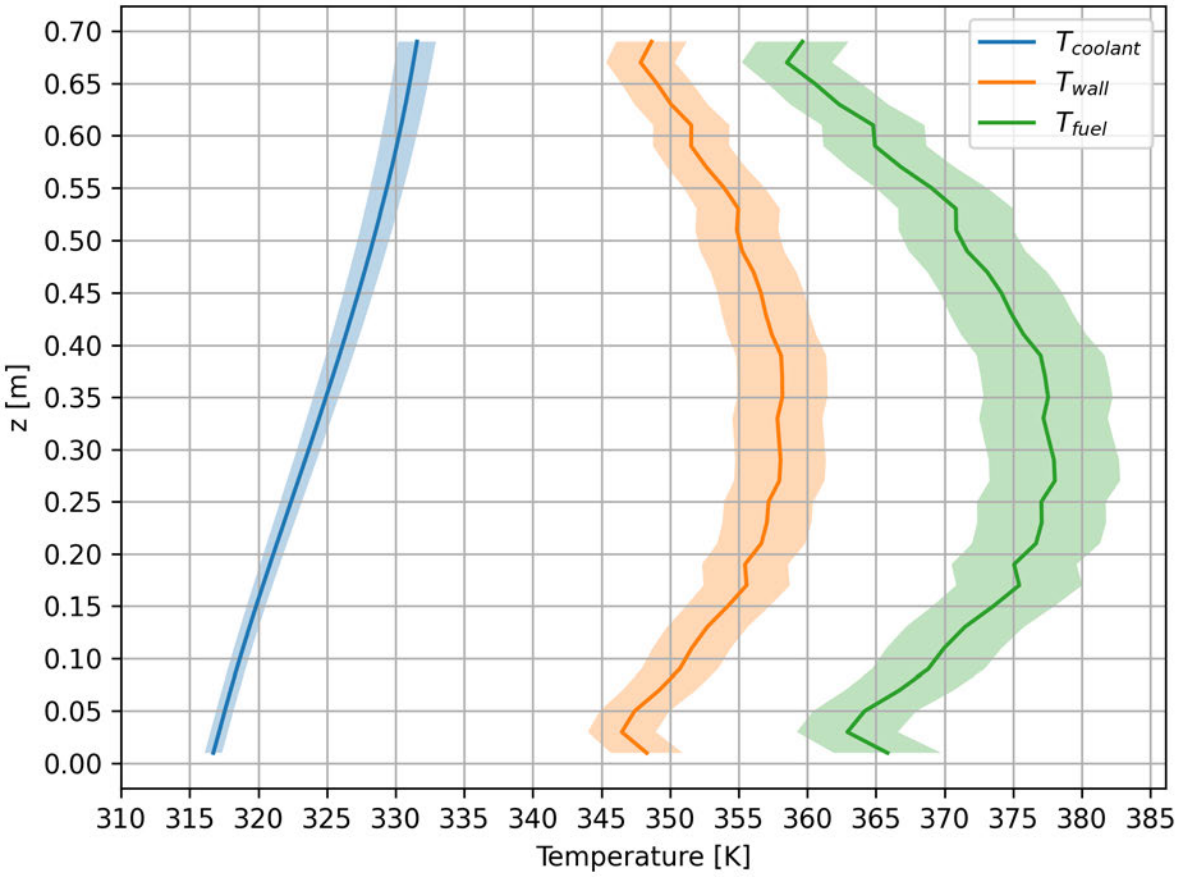

Figure 3. Axial distribution of temperature fields with uncertainty for the hottest channel at the BOC state

Similarly, uncertainty bounds of thermal limits are calculated for the 10,000 simulations. The mean values and uncertainty bounds of CHFR and OFIR are given in Table IV. The mean values of mCHFR and mOFIR are both above the 2.0 limit, with mCHFR being a more limiting factor than mOFIR.

Table IV. Mean thermal limits with their uncertainties at different core states

Core State	mCHFR	mOFIR
SU	2.19 ± 0.08	13.20 ± 0.63
BOC	2.14 ± 0.17	13.76 ± 0.63
MOC	2.38 ± 0.18	15.30 ± 0.69
EOC	2.60 ± 0.20	15.36 ± 1.43

To further analyze the distributions of mCHFR and mOFIR, their distributions are plotted on a histogram plot. The distribution of mCHFR is given in Figure 4. The limit of 2.0 is also plotted in the figure to visualize the proportion of the cases that exceeds the limit. Based on the distribution, it can be concluded that the probability of observing a mCHFR of less than 2.0 is calculated to be 4.2% for the steady-state operation of the NNS.

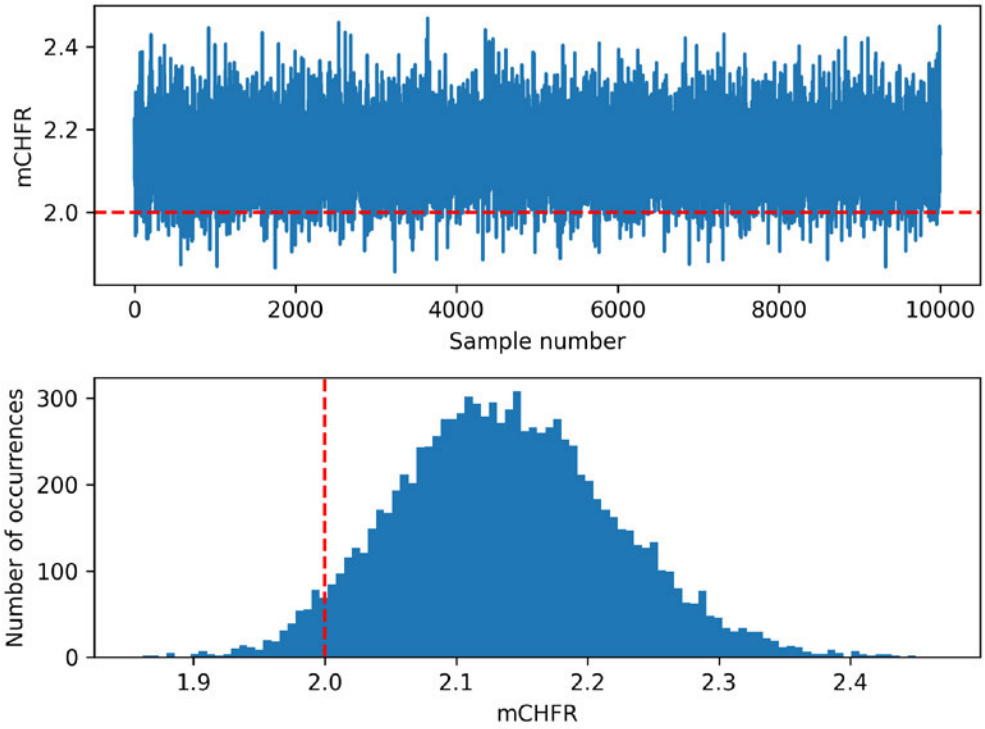

Figure 4. mCHFR distribution at BOC state

Similarly, the distribution of mOFIR is given in Figure 5. No cases were observed at which the mOFIR is below 2.0; therefore, mOFIR is not a limiting safety factor for the steady-state operation of the NNS. It is likely that other heat flux correlations can be used for calculating the mOFIR, but no other suitable correlations have been identified yet. The mOFIR not being a limiting parameter could imply to consider an additional thermal limit such as the onset of nucleate boiling. Future studies will further investigate these concerns.

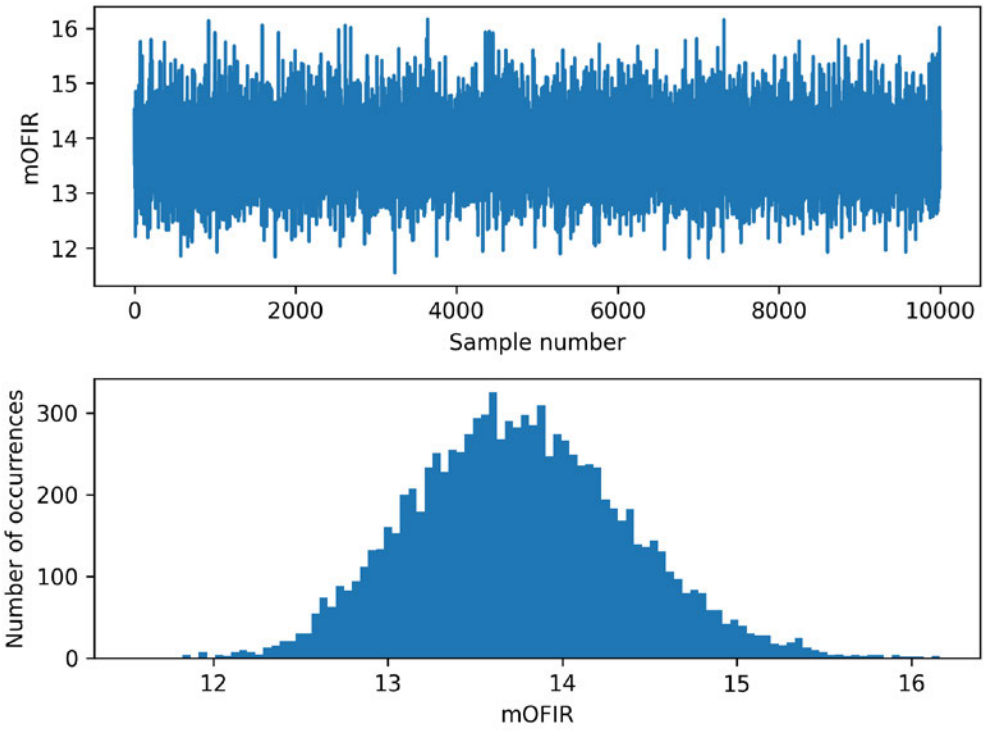

Figure 5. mOFIR distribution at BOC state

4. CONCLUSIONS

An in-house thermal-hydraulics analysis code was developed to assess the thermal-hydraulic characteristics of the proposed NIST Neutron Source design. The code is under development with the latest additions of heat conduction solver and uncertainty analysis tools. The temperature fields of bulk coolant, cladding wall, and fuel meat, and thermal limits such as minimum Critical Heat Flux Ratio (mCHFR) and minimum Onset of Flow Instability Ratio (mOFIR) are calculated and it is found that the addition of heat conduction affects the calculations 0.29% for maximum coolant temperature, 0.74% for maximum cladding wall temperature, 1.73% for mCHFR and 1.85% for mOFIR over all core states. Moreover, the uncertainty bounds of the temperature fields and thermal limits are calculated by running the code 10,000 times by sampling the core thermal power, total mass flow rate, and core inlet temperature. The probability distribution functions of sources of uncertainty are calculated considering the actual operation data of the NBSR. The statistical analysis confirms that the beginning of cycle is the most limiting cycle for the NNS, and the probability of observing the mCHFR is calculated to be 4.2% for the steady-state operation of the NNS.

ACKNOWLEDGMENTS

The authors would like to acknowledge helpful discussions with Dr. Lap-Yan Cheng from Brookhaven National Laboratory, and Idan Baroukh from the Nuclear Research Center in Negev. The identification of certain commercial equipment, instruments, or materials does not imply recommendation or endorsement by the authors or by the National Institute of Standards and Technology. Contributions of NIST are not subject to copyright in the United States.

REFERENCES

1. D. Şahin, et al., "NIST Neutron Source Preconceptual Design", *In RERTR 2022 – 42nd International Meeting on Reduced Enrichment for Research and Test Reactors*, October 3-5 (2022).
2. I.R. Baroukh, A. Gurgen, J.S. Shen, A.G. Weiss, "A Preliminary Thermal-hydraulics Analysis for the NIST Neutron Source", *Transactions of the American Nuclear Society*, ANS Winter Meeting, November 13-17 (2022).
3. A.G. Weiss, A. Gurgen, J. Shen, I.R. Baroukh, "Sensitivity Analyses of the Thermal-hydraulics Safety Margins in the Proposed NIST Neutron Source Design", *In Proceedings of the 30th International Conference on Nuclear Engineering*, Kyoto, Japan, May 21-26 (2023).
4. I.R. Baroukh, A. Gurgen, J.S. Shen, A.G. Weiss, "Preliminary CFD Investigations for the NIST Neutron Source", *Transactions of the American Nuclear Society*, ANS Winter Meeting, November 13-17 (2022).
5. A. Crabtree and M. Siman-Tov, "Thermophysical properties of saturated light and heavy water for Advanced Neutron Source applications," Oak Ridge National Lab., TN (United States), 1993.
6. B. Rabin et al, "Preliminary report on u-mo monolithic fuel for research reactors," Idaho National Laboratory INL/EXT-17-40975 (2017).
7. S. Polkinghorne and J. Lacy, "Thermophysical and Mechanical Properties of ATR Core Materials," EG&G Idaho Inc., Internal Technical Report, 1991
8. B.S. PETUKHOV, VV. KIRILLOV, "On the Question of Heat Transfer to a Turbulent Flow of Fluids in Pipes", *Teploenergetika (Thermal Engineering)* **4**, pp. 63-68 (1958).
9. S.W. CHURCHILL, "Friction-factor equation spans all fluid-flow regimes", *Chemical Engineering* **84** (24), pp. 91-92 (1977).
10. F. WHITE, *Fluid Mechanics*, 7th Ed., McGraw-Hill Series in Mechanical Engineering, New York, NY, USA (2009).
11. U.S. Nuclear Regulatory Commission, 1996, "Guidelines for preparing and reviewing applications for the licensing of non-power reactors: Standard review plan and acceptance criteria.," NUREG-1537 Pt.2, 211545.
12. M. Kaminaga, K. Yamamoto, Y. Sudo, "Improvement of Critical Heat Flux Correlation for Research Reactors using Plate-Type Fuel", *Journal of Nuclear Science and Technology,* **35(12)**, 943-951 (1998).
13. P. Saha, N. Zuber, "Point of net vapor generation and vapor void fraction in subcooled boiling", *Proceedings of the 5th International Heat Transfer Conference,* **4** (1974).
14. O.S. Celikten, D. Sahin, A.G. Weiss, 2022, "Highlights of Neutronic Analyses for the Pre-conceptual NIST Neutron Source Design," *Transactions of the American Nuclear Society*, ANS Winter Meeting, November 13-17 (2022).
15. D.B. Owen, *Handbook of Statistical Tables*, Addison-Wesley, Massachusetts, USA (1962).